Submitted to

23rd International Symposium on Lepton-Photon Interactions at High Energy, LP2007,
August 13-18, 2007, Daegu, Republic of Korea.

Electronic Access: www-h1.desy.de/h1/www/publications/conf/conf_list.html

H1prelim-07-171
August 2007

Measurement of $F_2^{c\bar{c}}$ and $F_2^{b\bar{b}}$ using the H1 Vertex Detector at HERA

H1 Collaboration

Abstract

The inclusive charm and beauty cross sections are measured in $e^{-}p$ collisions at HERA in the kinematic region of photon virtuality $12 \leq Q^2 \leq 650\ \mathrm{GeV}^2$ and Bjorken scaling variable $0.0002 \leq x \leq 0.032$. The data were collected with the H1 detector in 2006 corresponding to an integrated luminosity of $54\ \mathrm{pb}^{-1}$. The charm and beauty fractions are determined using a method based on the impact parameter, in the transverse plane, of tracks to the primary vertex, as measured by the H1 vertex detector. The measurements are compared with previous data and NLO predictions.

1 Introduction

In this paper measurements of the charm (c) and beauty (b) contributions to the inclusive proton structure function F_2 are made in Deep Inelastic Scattering (DIS) at HERA, using information from the H1 vertex detector, for values of the negative square of the four momentum of the exchanged boson $12 \leq Q^2 \leq 650\ \mathrm{GeV}^2$, and of Bjorken x, $0.000197 \leq x \leq 0.032$. The analysis is based on a sample of $e^- p$ neutral current scattering events corresponding to an integrated luminosity of $54\ \mathrm{pb}^{-1}$, taken in the year 2006, at an ep centre of mass energy $\sqrt{s} = 319\ \mathrm{GeV}$, with a proton beam energy of $920\ \mathrm{GeV}$. The analysis method employed is similar to that used by H1 in measurements of HERA-I data [1, 2].

Events containing heavy quarks are distinguished from those containing only light quarks by reconstructing the displacement of tracks from the primary vertex, using precise spatial information from the H1 vertex detector. The long lifetimes of c and b flavoured hadrons lead to larger displacements than for light quark events. The charm structure function $F_2^{c\bar{c}}$ and the beauty structure function $F_2^{b\bar{b}}$ are obtained from the measured c and b cross sections after small corrections for the longitudinal structure functions $F_L^{c\bar{c}}$ and $F_L^{b\bar{b}}$.

2 Monte Carlo Simulation

Monte Carlo simulations are used to correct for the effects of the finite detector resolution, acceptance and efficiency. The Monte Carlo program RAPGAP [3] is used to generate DIS events for the processes $ep \to eb\bar{b}X$, $ep \to ec\bar{c}X$ and $ep \to eqX$ where q is a light quark of flavour u, d or s. The Monte Carlo program CASCADE [4] is also used to produce b and c events. RAPGAP combines $\mathcal{O}(\alpha_s)$ matrix elements with higher order QCD effects modelled by the emission of parton showers. The heavy flavour event samples are generated according to the massive photon gluon fusion (PGF) matrix element with the mass of the c and b quarks set to $m_c = 1.5\ \mathrm{GeV}$ and $m_b = 4.75\ \mathrm{GeV}$, respectively. The DIS cross section is calculated using the leading order (LO) 3-flavour parton distribution functions (PDFs) from [6]. CASCADE is an implementation of the CCFM [5] evolution equation and uses off shell matrix elements convoluted with k_t unintegrated proton parton distributions.

The partonic system for all generated events is fragmented according to the LUND string model implemented within the PYTHIA program [7]. The HERACLES program [8] calculates single photon radiative emissions off the lepton line, virtual and electroweak corrections.

The samples of events generated for the uds, c, and b processes are passed through a detailed simulation of the detector response based on the GEANT3 program [9], and through the same reconstruction software as is used for the data. We use all b and c event statistics from both RAPGAP and CASCADE to compare with and correct the data.

3 H1 Detector

Only a short description of the H1 detector is given here; a full description may be found in [10]. A right handed coordinate system is employed at H1 that has its z-axis pointing in the proton beam, or forward, direction and x (y) pointing in the horizontal (vertical) direction.

Charged particles are measured in the central tracking detector (CTD). This device consists of two cylindrical drift chambers interspersed with z-chambers to improve the z-coordinate reconstruction and multi–wire proportional chambers mainly used for triggering. The CTD is situated in a uniform $1.15\,\mathrm{T}$ magnetic field, enabling momentum measurement of charged particles over the polar angular range[1] $20^\circ < \theta < 160^\circ$.

The CTD tracks are linked to hits in the vertex detector (central silicon tracker CST) [11] to provide precise spatial track reconstruction. The CST consists of two layers of double-sided silicon strip detectors surrounding the beam pipe, covering an angular range of $30^\circ < \theta < 150^\circ$ for tracks passing through both layers. The information on the z-coordinate of the CST tracks is not used in the analysis presented in this paper. For CTD tracks with CST hits in both layers the transverse distance of closest approach (DCA) to the nominal vertex in x–y can be measured with a resolution of $33\ \mu\mathrm{m} \oplus 90\ \mu\mathrm{m}/p_T[\mathrm{GeV}]$, where the first term represents the intrinsic resolution (including alignment uncertainty) and the second term is the contribution from multiple scattering in the beam pipe and the CST; p_T is the transverse momentum of the track.

The track detectors are surrounded in the forward and central directions ($4^\circ < \theta < 155^\circ$) by a fine grained liquid argon calorimeter (LAr) and in the backward region ($153^\circ < \theta < 178^\circ$) by a lead–scintillating fibre calorimeter (SPACAL) [12] with electromagnetic and hadronic sections. These calorimeters provide energy and angular reconstruction for final state particles from the hadronic system and are also used in this analysis to measure and identify the scattered electron.

Electromagnetic calorimeters situated downstream in the electron beam direction allow detection of photons and electrons scattered at very low Q^2. The luminosity is measured from the rate of photons produced in the Bethe-Heitler process $ep \rightarrow ep\gamma$.

4 Experimental Method

4.1 Event and Track Selection

The events are selected by requiring a compact electromagnetic cluster in either the LAr or SPACAL calorimeters. The z position of the interaction vertex, reconstructed by one or more charged tracks in the tracking detectors, must be within ± 20 cm of the centre of the detector to match the acceptance of the CST. Photoproduction events are suppressed by requiring $\sum_i (E_i - p_{z,i}) > 35$ GeV. Here, E_i and $p_{z,i}$ denote the energy and longitudinal momentum components of a particle and the sum is over all final state particles including the scattered electron and the hadronic final state (HFS). The HFS particles are reconstructed using a combination of tracks and calorimeter deposits in an energy flow algorithm that avoids double counting. The event kinematics, Q^2 and the inelasticity variable y, are reconstructed with the '$e\Sigma$' method [13], which uses the scattered electron and the HFS. The Bjorken scaling variable x is obtained from $x = Q^2/sy$. In order to have good acceptance in the SPACAL and to ensure that the HFS has a significant transverse momentum, events are selected in the range $6.3 < Q^2 < 1585\ \mathrm{GeV}^2$. The analysis is restricted to $0.07 < y < 0.625$ to ensure that the direction of the quark which

[1] The angular coverage of each detector component is given for the interaction vertex in its nominal position.

is struck by the photon is mostly in the CST angular range and to reduce photoproduction background.

The position of the beam interaction region, calculated at regular time intervals using information from tracks with CST hits, is used as the position of the primary event vertex in r–ϕ. The impact parameter of a track, which is the transverse distance of closest approach (DCA) of the track to the primary vertex point, is only determined for those tracks which are measured in the CTD and have at least one CST hit linked (referred to as CST tracks). Only CST tracks with a transverse momentum > 0.5 GeV are included in the DCA and related distributions that are used to separate the different quark flavours.

In order to determine a signed impact parameter (δ) for a track, the azimuthal angle of the struck quark ϕ_{quark} must be determined for each event. To do this, jets with a minimum p_T of 1.5 GeV, in the angular range $15^\circ < \theta < 155^\mathrm{o}$, are reconstructed using the invariant k_T algorithm [14] in the laboratory frame using all reconstructed HFS particles. The angle ϕ_{quark} is defined as the ϕ of the jet with the highest transverse momentum or, if there is no jet reconstructed in the event, as $180^\circ - \phi_{\mathrm{elec}}$, where ϕ_{elec} is the azimuthal angle of the electron in degrees. The direction defined in the transverse plane by ϕ_{quark} and the primary vertex is called the quark axis. Approximately 95% (99%) of c (b) events have ϕ_{quark} reconstructed from a jet, as determined from the Monte Carlo simulation.

If the angle between the quark axis and the line joining the primary vertex to the point of DCA is less than 90°, δ is defined as positive, and is defined as negative otherwise. Tracks with azimuthal angle outside $\pm 90^\circ$ of ϕ_{quark} are rejected. The δ distribution, shown in figure 1, is seen to be asymmetric with positive values in excess of negative values indicating the presence of long lived particles. It is found to be well described by the Monte Carlo simulation. Tracks with $|\delta| > 0.1$ cm are rejected from the analysis to suppress light quark events containing long lived strange particles.

4.2 Quark Flavour Separation

The method used in [1] to distinguish between the c, b and light quark flavours is used in the present analysis. The quantities S_1 and S_2 are defined as the significance ($\delta/\sigma(\delta)$) of the track with the highest and second highest absolute significance, respectively, where $\sigma(\delta)$ is the error on δ. Distributions of S_1 for events with only 1 reconstructed CST track and S_2 for events with $\geq$ 2 reconstructed CST tracks are made. Events in which S_1 and S_2 have opposite signs are excluded from the S_2 distribution. Figure 2 shows the significance distributions. The simulation gives a reasonable description of the data.

In order to reduce the uncertainty due to the resolution of δ and the light quark normalisation, the contents of the negative bins in the significance distributions are subtracted from the contents of the corresponding positive bins. The subtracted distributions are shown in figure 3. It can be seen that the resulting distributions are dominated by c quark events, with a b fraction increasing with significance. The light quarks contribute a small fraction for all values of significance.

The fractions of c, b and light quarks of the data are extracted in each x–Q^2 interval using a least squares simultaneous fit to the subtracted S_1 and S_2 distributions (as in figure 3) and the total number of inclusive events before any CST track selection. The c, b and uds Monte Carlo simulation samples are used as templates. The Monte Carlo c, b and uds contributions in each x–Q^2 interval are scaled by factors P_c, P_b and P_l, respectively, to give the best fit to the observed subtracted S_1 and S_2 and total distributions. Only the statistical errors of the data and Monte Carlo simulation are considered in the fit. The fit to the subtracted significance distributions mainly constrains P_c and P_b, whereas the overall normalisation constrains P_l.

The results of the fit to the complete data sample are shown in figure 3. The fit gives a good description of all the significance distributions, with a $\chi^2/n.d.f$ of $26.2/31$. Values of $P_c = 0.97 \pm 0.02$, $P_b = 0.86 \pm 0.08$ and $P_l = 1.062 \pm 0.005$ are obtained. The c and b scale factors are found to be anti-correlated with an overall correlation coefficient of -0.72. Acceptable χ^2 values are also found for the fits to the samples in the separate x–Q^2 intervals.

The results of the fit in each x–Q^2 interval are converted to a measurement of the 'reduced c cross section' defined from the differential cross section as

$$\tilde{\sigma}^{c\bar{c}}(x,Q^2) = \frac{\mathrm{d}^2\sigma^{c\bar{c}}}{\mathrm{d}x\,\mathrm{d}Q^2}\frac{xQ^4}{2\pi\alpha^2(1+(1-y)^2)}, \tag{1}$$

using:

$$\tilde{\sigma}^{c\bar{c}}(x,Q^2) = \tilde{\sigma}(x,Q^2)\frac{P_c N_c^{\mathrm{MCgen}}}{P_c N_c^{\mathrm{MCgen}} + P_b N_b^{\mathrm{MCgen}} + P_l N_l^{\mathrm{MCgen}}}\delta_{\mathrm{BCC}}, \tag{2}$$

where $\tilde{\sigma}(x,Q^2)$ is the measured inclusive reduced cross section from H1([15] for $Q^2 \leq 60\ \mathrm{GeV}^2$, otherwise [16]) and N_c^{MCgen}, N_b^{MCgen} and N_l^{MCgen} are the number of c, b and light quark events generated from the Monte Carlo in each bin. A bin centre correction δ_{BCC} is applied using a NLO QCD expectation for $\tilde{\sigma}^{c\bar{c}}$ to convert the bin averaged measurement into a measurement at a given x–Q^2 point. The NLO QCD expectation is calculated from the results of a fit similar to that performed in [17] but using the FFNS scheme to generate heavy flavours. A small correction ($\leq 2.6\%$) for the beam energy difference is applied, using the NLO QCD expectation, to the measurement of $\tilde{\sigma}(x,Q^2)$ with $Q^2 \leq 60\ \mathrm{GeV}^2$ which was performed at a lower centre of mass energy of $301\ \mathrm{GeV}$ than the data presented here. The cross section is defined so as to include a correction for pure QED radiative effects. Events that contain c hadrons via the decay of b hadrons are not included in the definition of the c cross section. The differential b cross section is evaluated in the same manner.

5 Results

The measurements, shown as a function of x for fixed values of Q^2, of $\tilde{\sigma}^{c\bar{c}}$ are shown in figure 4 and of $\tilde{\sigma}^{b\bar{b}}$ in figure 5. Also shown in these figures are the HERA I data extracted using the displaced track method. All data show good agreement for both $\tilde{\sigma}^{c\bar{c}}$ and $\tilde{\sigma}^{b\bar{b}}$ for all measured x and Q^2 values. We therefore average the results using the method of [18]. In this method the correlation between the systematic errors of the data points are taken into account. The averaged measurements are also shown in figures figure 4 and 5.

The measurement of $\tilde{\sigma}^{c\bar{c}}$ are compared in figure 6 with those extracted from D^* meson measurements by H1 [19] and ZEUS [20], obtained using a NLO program [21] based on DGLAP evolution to extrapolate the measurements outside the visible D^* range. The measurements for $\tilde{\sigma}^{c\bar{c}}$ from the present analysis, the HERA I data and the D^* extraction methods are in good agreement.

The $\tilde{\sigma}^{c\bar{c}}$ data are compared with two predictions from NLO QCD based on the variable flavour number scheme (VFNS) from MRST [22] and CTEQ [23], and with predictions based on CCFM [5] parton evolution. The predictions provide a reasonable description of the present data.

The $\tilde{\sigma}^{b\bar{b}}$ data are compared in figure 7 as a function of x for fixed values of Q^2 with the two VFNS NLO QCD predictions and the CCFM prediction. The difference between the two VFNS NLO QCD calculations, which reaches a factor 2 at the lowest Q^2 and x, arises from the different treatments of threshold effects by MRST and CTEQ. The data are compared with ZEUS data [24] in figure 8. The ZEUS cross sections are derived from events with a jet and a muon, and Monte Carlo models used to extrapolate over unseen phase space. The ZEUS data are somewhat higher than the H1 measurements.

The structure function $F_2^{c\bar{c}}$ is evaluated from the reduced cross section

$$\tilde{\sigma}^{c\bar{c}} = F_2^{c\bar{c}} - \frac{y^2}{1+(1-y)^2} F_L^{c\bar{c}}, \tag{3}$$

where the longitudinal structure function $F_L^{c\bar{c}}$ is estimated from the same NLO QCD expectation as used for the bin centre correction. The structure function $F_2^{b\bar{b}}$ is evaluated in the same manner.

The measurements $F_2^{c\bar{c}}$ and $F_2^{b\bar{b}}$ are shown as a function of Q^2 in figure 9 and figure 10. The $F_2^{b\bar{b}}$ values are compared with the ZEUS measurements in figure 11. The data are compared with the VFNS QCD predictions from MRST and CTEQ at NLO and a recent calculation at NNLO [25].

6 Conclusion

The differential charm and beauty cross sections in Deep Inelastic Scattering are measured for a wide range of Q^2 and Bjorken x using the impact parameters of tracks from decays of long lived c and b hadrons as reconstructed from the vertex detector, using a part of the HERA II data. The cross sections and derived structure functions $F_2^{c\bar{c}}$ and $F_2^{b\bar{b}}$ are found to agree with previous measurements and be described by by predictions of perturbative QCD. A combination of the HERA I data with the HERA II data has been performed resulting in a more precise measurement.

References

[1] A. Aktas *et al.* [H1 Collaboration], Eur. Phys. J. C **40** (2005) 349 [hep-ex/0411046].

[2] A. Aktas *et al.* [H1 Collaboration], Eur. Phys. J. C **45** (2006) 23 [arXiv:hep-ex/0507081].

[3] H. Jung, Comput. Phys. Commun. **86** (1995) 147;
(see also http://www.desy.de/∼jung/rapgap/).

[4] H. Jung and G. P. Salam, Eur. Phys. J. C **19** (2001) 351 [hep-ph/0012143];

[5] M. Ciafaloni, Nucl. Phys. B **296** (1988) 49;
S. Catani, F. Fiorani and G. Marchesini, Phys. Lett. B **234** (1990) 339;
S. Catani, F. Fiorani and G. Marchesini, Nucl. Phys. B **336** (1990) 18;
G. Marchesini, Nucl. Phys. B **445** (1995) 49 [hep-ph/9412327].

[6] A. D. Martin, W. J. Stirling and R. S. Thorne, Phys. Lett. B **636** (2006) 259 [arXiv:hep-ph/0603143].

[7] T. Sjostrand, L. Lonnblad and S. Mrenna, arXiv:hep-ph/0108264.

[8] A. Kwiatkowski, H. Spiesberger and H. J. Möhring, Comput. Phys. Commun. **69** (1992) 155.

[9] R. Brun, R. Hagelberg, M. Hansroul and J. C. Lassalle, CERN-DD-78-2-REV.

[10] I. Abt *et al.* [H1 Collaboration], Nucl. Instrum. Meth. A **386** (1997) 310 and 348.

[11] D. Pitzl *et al.*, Nucl. Instrum. Meth. A **454** (2000) 334 [hep-ex/0002044].

[12] T. Nicholls *et al.* [H1 SPACAL Group], Nucl. Instrum. Meth. A **374** (1996) 149.

[13] U. Bassler and G. Bernardi, Nucl. Instrum. Meth. A **361** (1995) 197 [hep-ex/9412004];

[14] S. D. Ellis and D. E. Soper, Phys. Rev. D **48** (1993) 3160 [hep-ph/9305266];
S. Catani, Y. L. Dokshitzer, M. H. Seymour and B. R. Webber, Nucl. Phys. B **406** (1993) 187.

[15] C. Adloff *et al.* [H1 Collaboration], Eur. Phys. J. C **21** (2001) 33 [hep-ex/0012053].

[16] C. Adloff *et al.* [H1 Collaboration], Eur. Phys. J **C 30** (2003) 1 [hep-ex/0304003].

[17] C. Adloff *et al.* [H1 Collaboration], Eur. Phys. J. C **13** (2000) 609 [hep-ex/9908059].

[18] A. Glazov, AIP Conf. Proc. **792** (2005) 237.

[19] C. Adloff *et al.* [H1 Collaboration], Phys. Lett. B **528** (2002) 199 [hep-ex/0108039].

[20] S. Chekanov *et al.* [ZEUS Collaboration], Phys. Rev. D **69** (2004) 012004 [hep-ex/0308068].

[21] B. W. Harris and J. Smith, Phys. Rev. D **57** (1998) 2806 [hep-ph/9706334].

[22] A. D. Martin, R. G. Roberts, W. J. Stirling and R. S. Thorne, Eur. Phys. J. C **39** (2005) 155 [hep-ph/0411040].

[23] S. Kretzer, H. L. Lai, F. I. Olness and W. K. Tung, Phys. Rev. D **69** (2004) 114005 [hep-ph/0307022].

H. Jung, Comput. Phys. Commun. **143** (2002) 100 [hep-ph/0109102];
(see also http://www.desy.de/∼jung/cascade/).

[24] ZEUS Collaboration, "Measurement of $F_2^{b\bar{b}}$ at HERA II", contribution to the HEP2007 International Europhysics Conference on High Energy Physics, Manchester UK, July 2007.

[25] R. Thorne, "A Variable Flavour Number Scheme at NNLO," To appear in the proceedings of 13^{th} International Workshop on Deep Inelastic Scattering (DIS 2005), Madison, Wisconsin, USA, April 2005. [hep-ph/0506251].

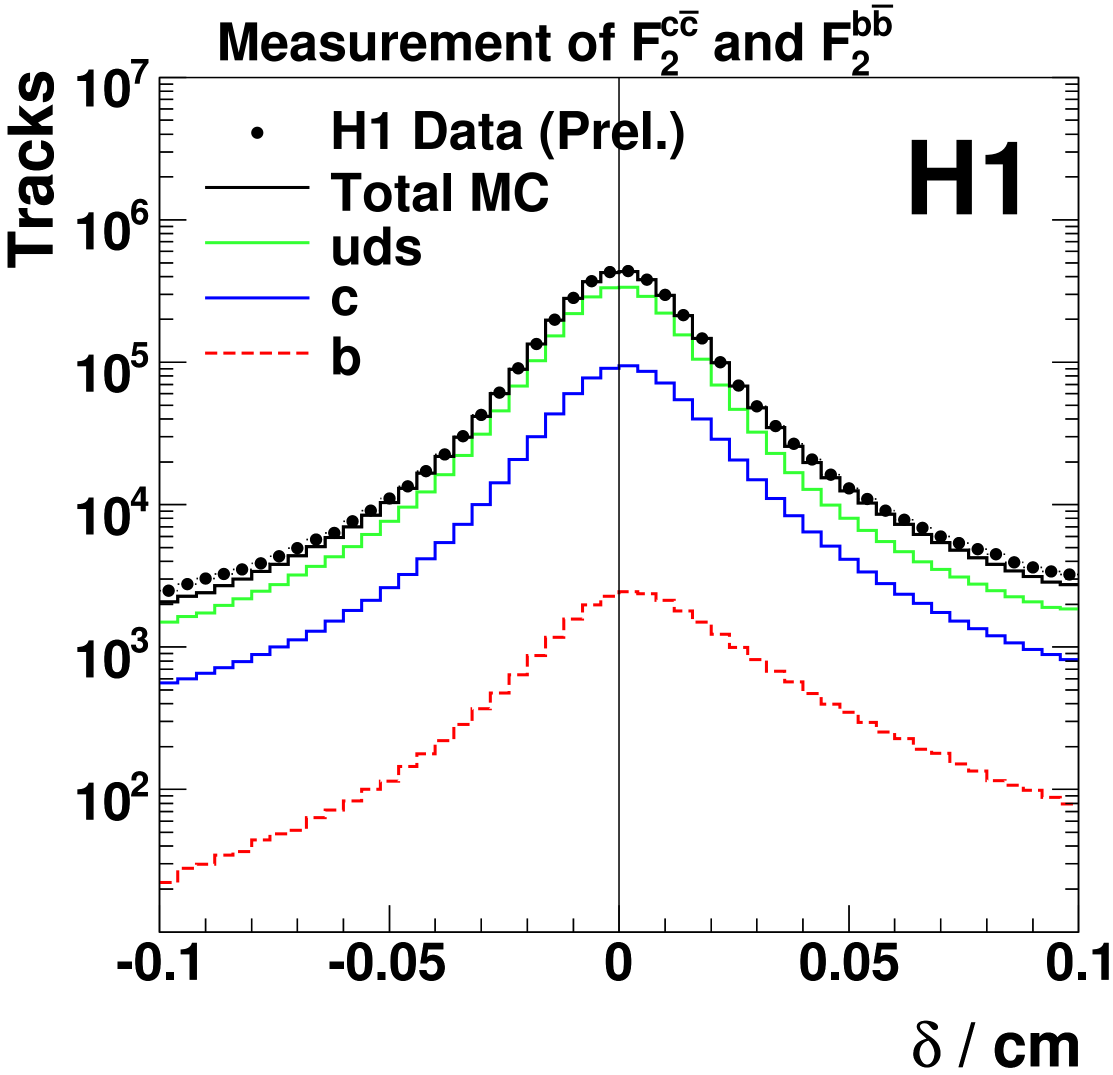

Figure 1: The distribution of the signed impact parameter δ of a track to the primary vertex in the x–y plane. Included in the figure is the expectation from the Monte Carlo simulation for light, c and b quarks. The contributions from the various quark flavours are shown after applying the scale factors obtained from the fit to the subtracted significance distributions of the data (see section 4.2).

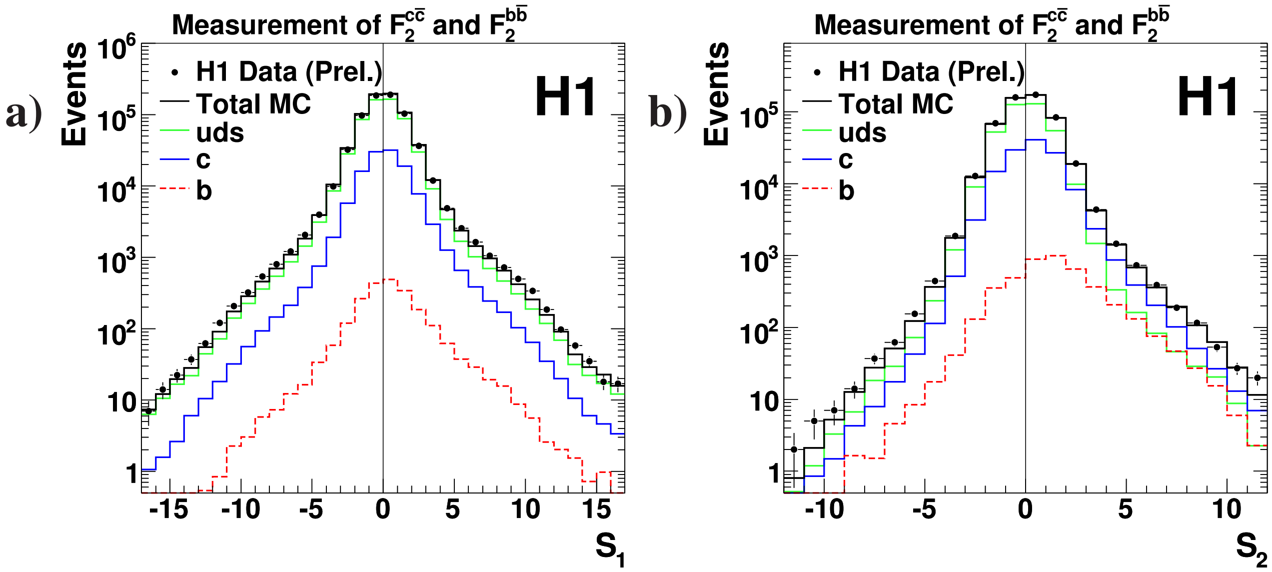

Figure 2: The significance $\delta/\sigma(\delta)$ distribution (a) of the highest absolute significance track (S_1) for 1 track events and (b) of the track with the second highest absolute significance (S_2). Included in the figure is the expectation from the Monte Carlo simulation for light, c and b quarks. The contributions from the various quark flavours are shown after applying the scale factors obtained from the fit to the subtracted significance distributions of the data.

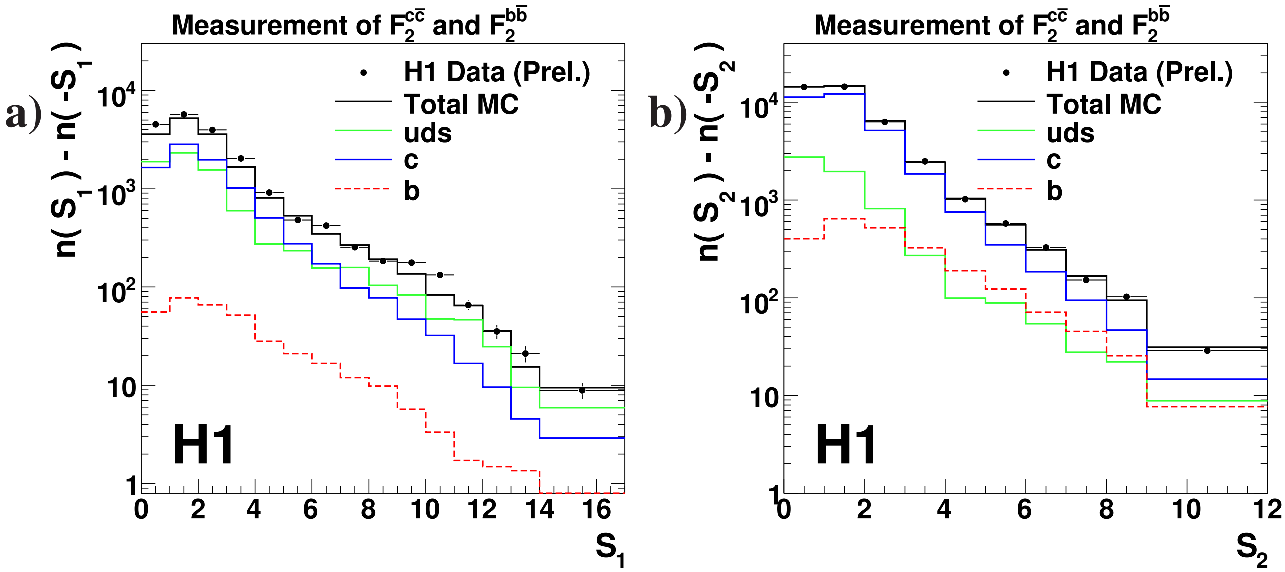

Figure 3: The subtracted significance distributions of (a) S_1 for 1 track events and (b) S_2. Included in the figure is the result from the fit to the data of the Monte Carlo distributions of the various quark flavours.

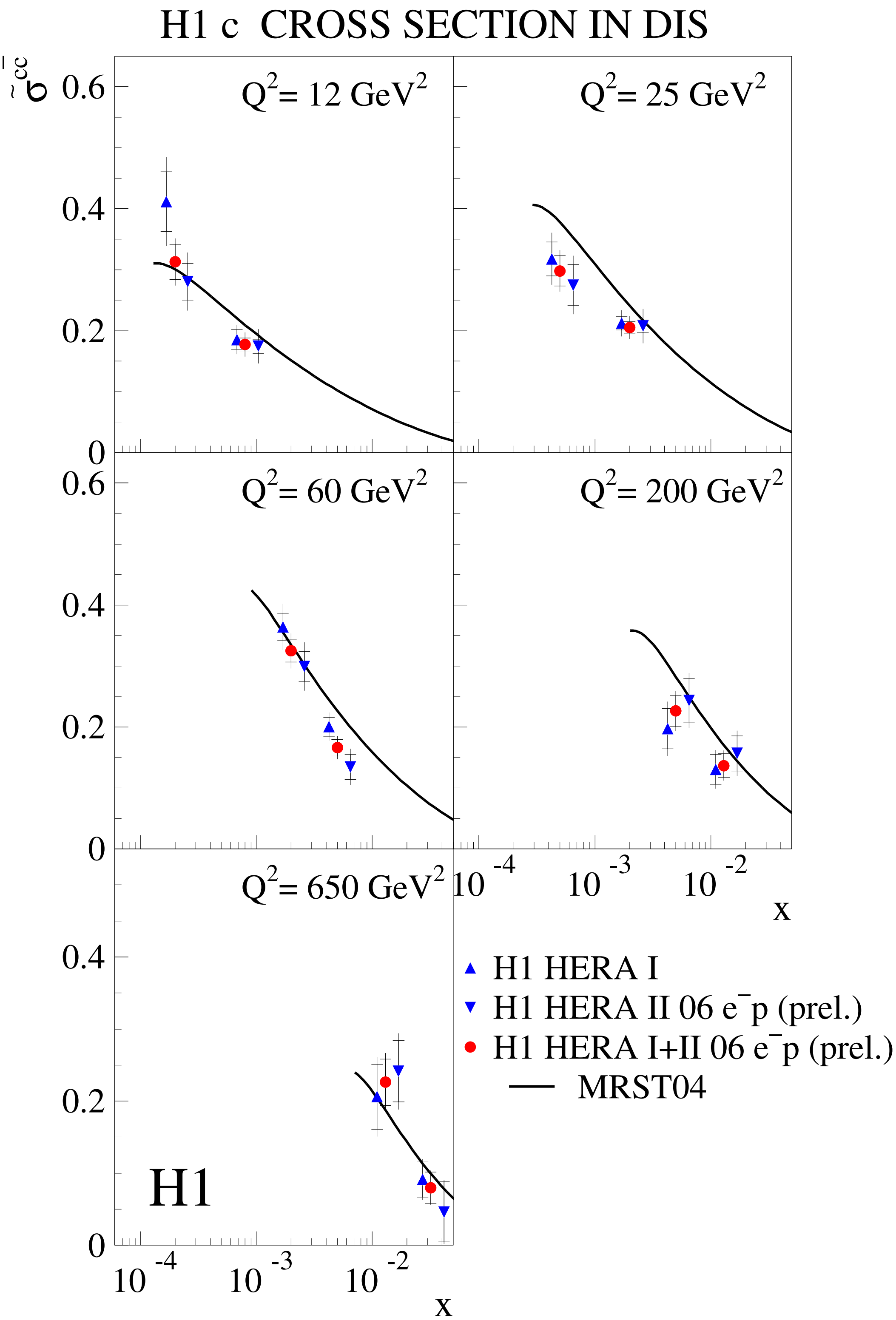

Figure 4: The measured reduced cross section $\tilde{\sigma}^{c\bar{c}}$ shown as a function of x for 5 different Q^2 values. The inner error bars show the statistical error, the outer error bars represent the statistical and systematic errors added in quadrature. The measurements are compared with those from HERA I, and the HERA I and II averaged data are also shown.

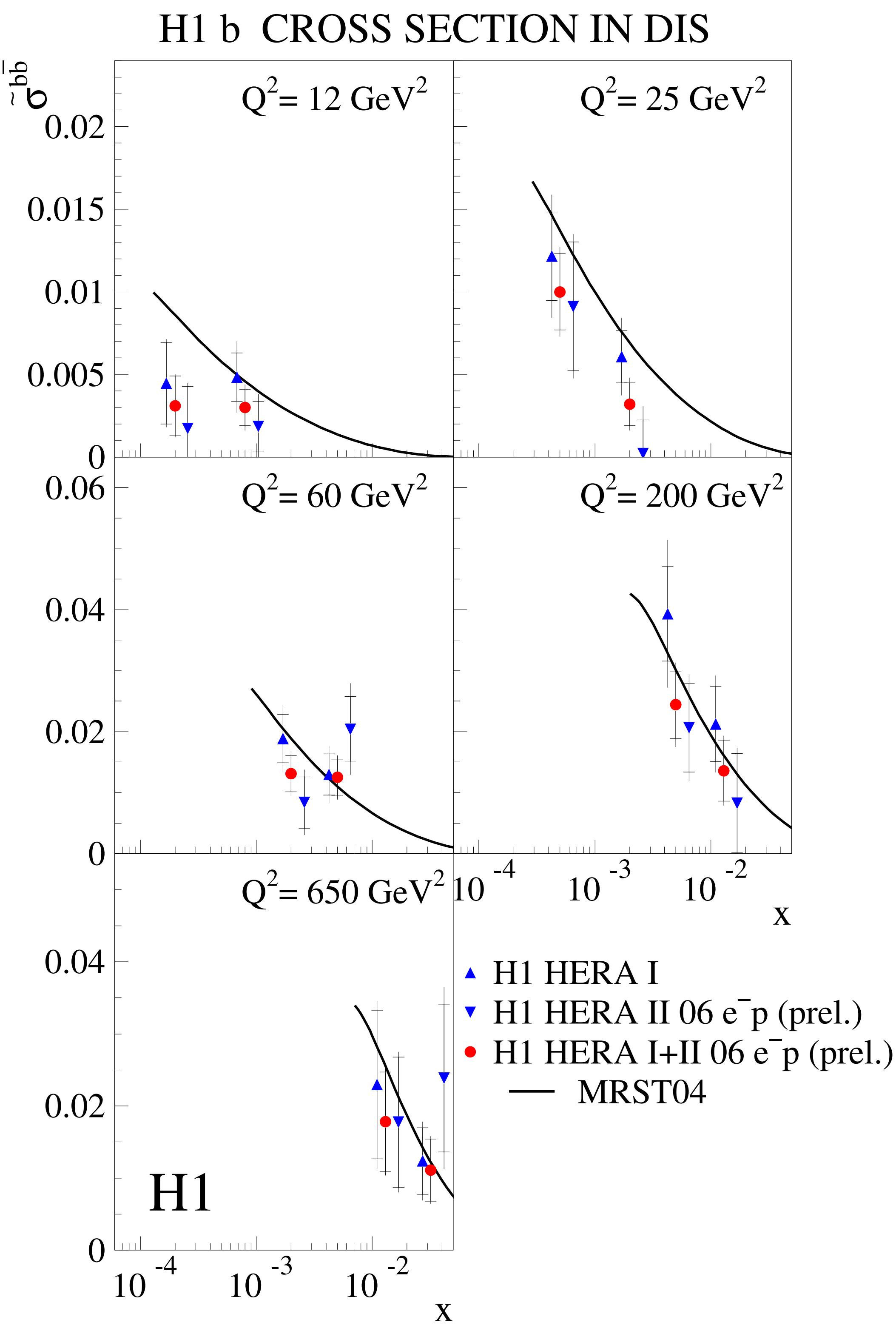

Figure 5: The measured reduced cross section $\tilde{\sigma}^{b\bar{b}}$ shown as a function of x for 5 different Q^2 values. The inner error bars show the statistical error, the outer error bars represent the statistical and systematic errors added in quadrature. The measurements are compared with those from HERA I, and the HERA I and HERA II averaged data are also shown.

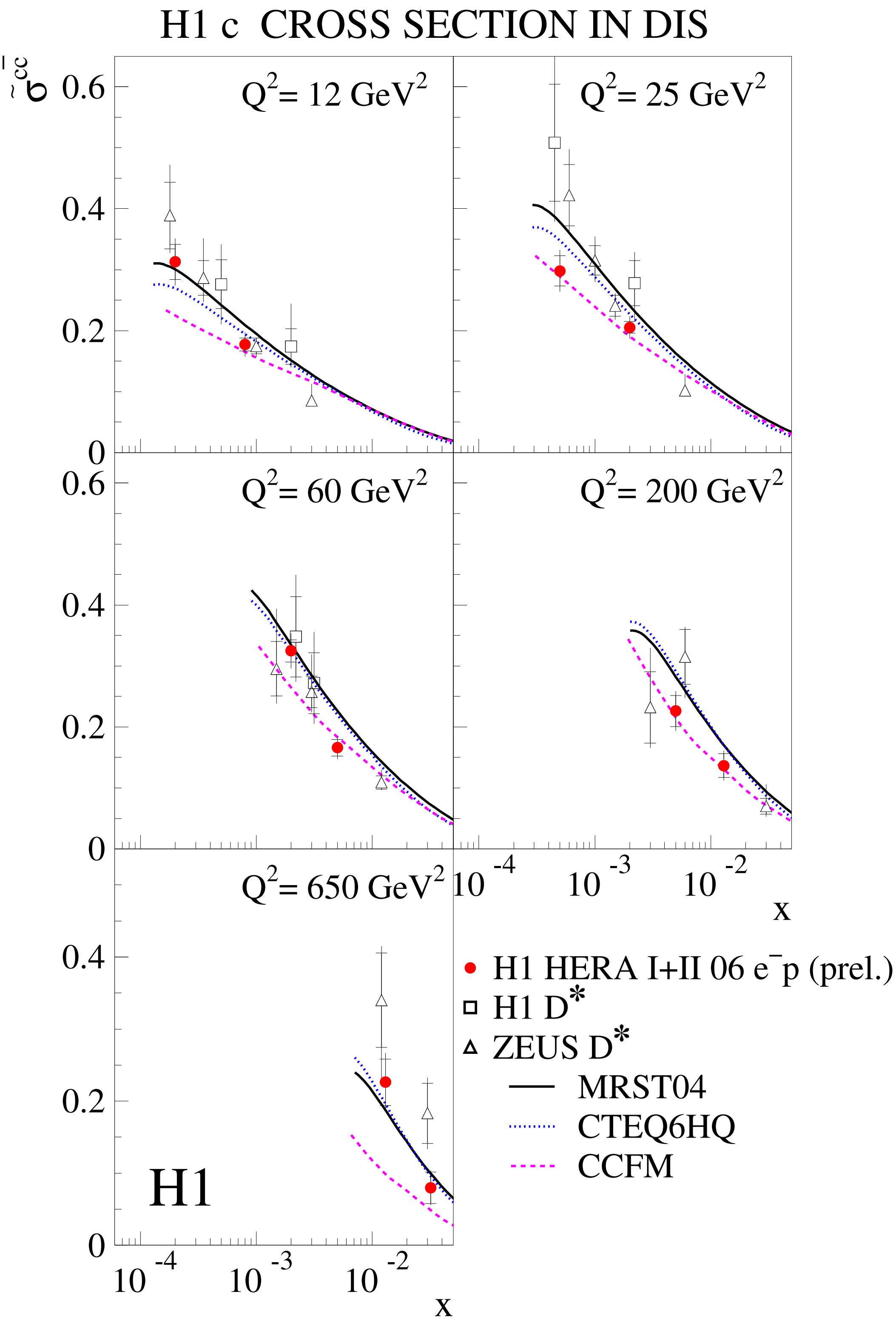

Figure 6: The measured HERA I and II averaged reduced cross section $\tilde{\sigma}^{c\bar{c}}$ shown as a function of x for 5 different Q^2 values. The inner error bars show the statistical error, the outer error bars represent the statistical and systematic errors added in quadrature. The measurements obtained from D^* mesons from H1 and ZEUS [19, 20] and predictions of QCD are also shown.

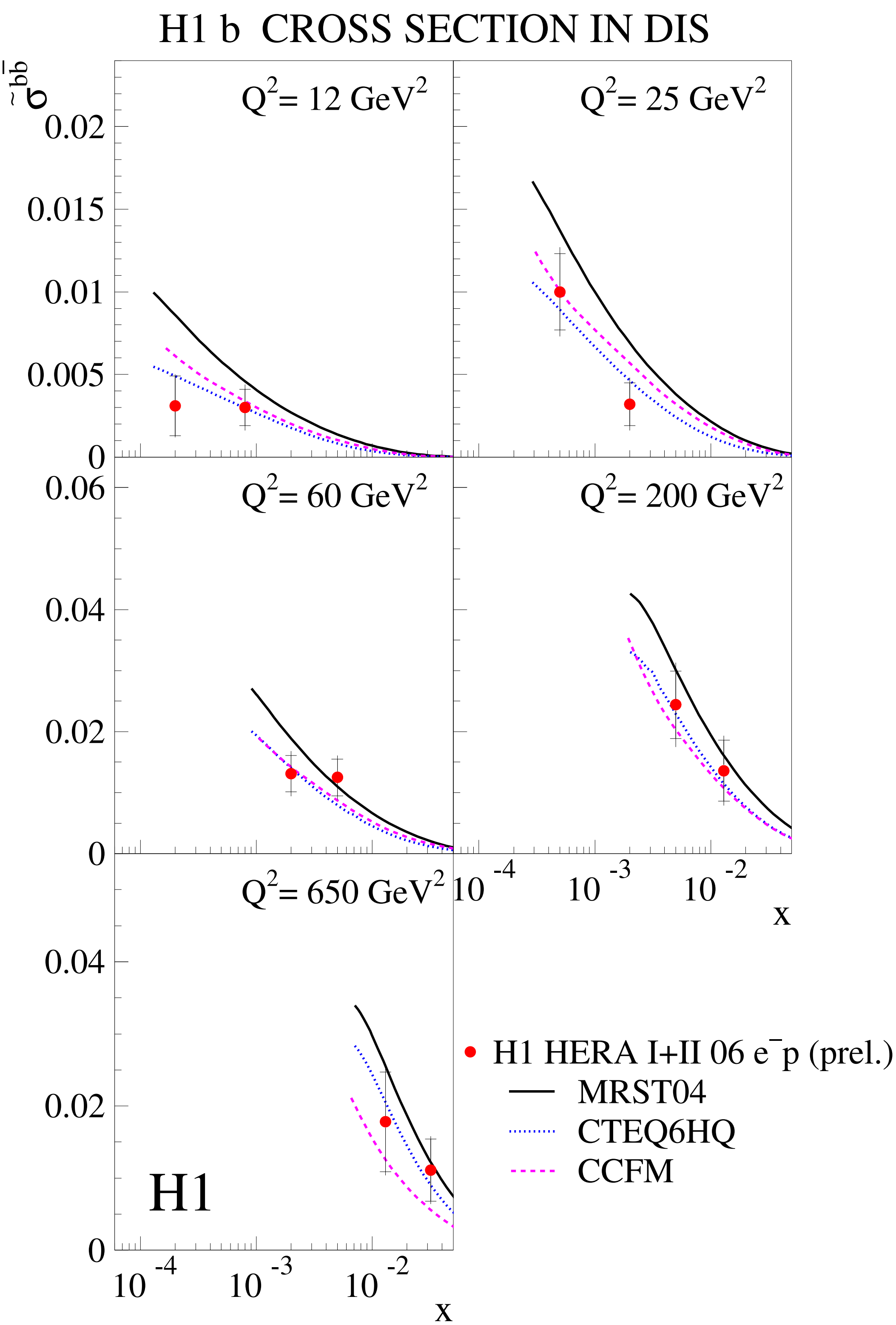

Figure 7: The measured HERA I and II averaged reduced cross section $\tilde{\sigma}^{b\bar{b}}$ shown as a function of x for 5 different Q^2 values. The inner error bars show the statistical error, the outer error bars represent the statistical and systematic errors added in quadrature. The predictions of QCD are also shown.

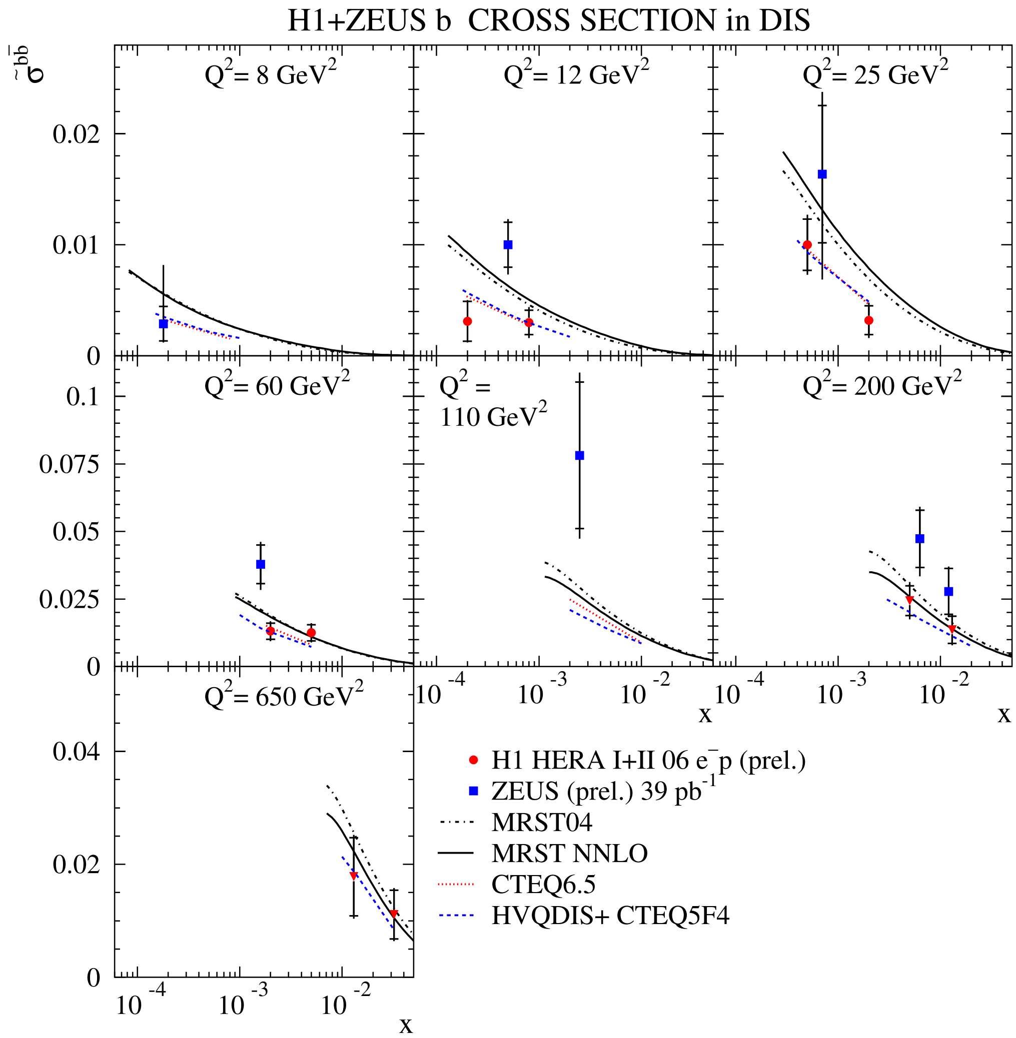

Figure 8: The measured HERA I and II averaged reduced cross section $\tilde{\sigma}^{b\bar{b}}$ shown as a function of x for 5 different Q^2 values. The inner error bars show the statistical error, the outer error bars represent the statistical and systematic errors added in quadrature. The preliminary data from ZEUS and the predictions of QCD are also shown.

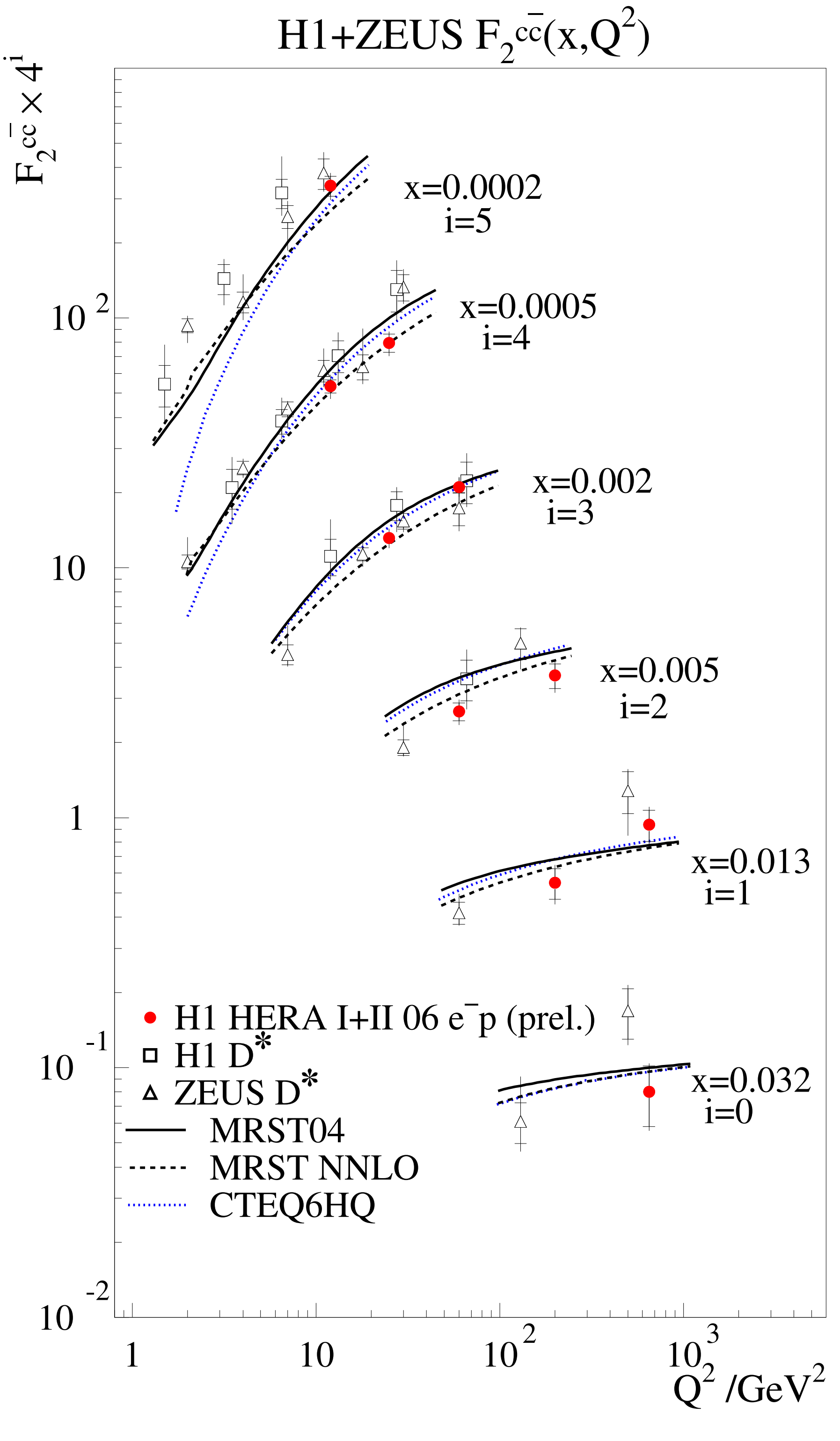

Figure 9: The measured HERA I and II averaged $F_2^{c\bar{c}}$ shown as a function of Q^2 for various x values. The inner error bars show the statistical error, the outer error bars represent the statistical and systematic errors added in quadrature. The measurements obtained from D^* mesons from H1 and ZEUS [19, 20] and predictions of QCD are also shown.

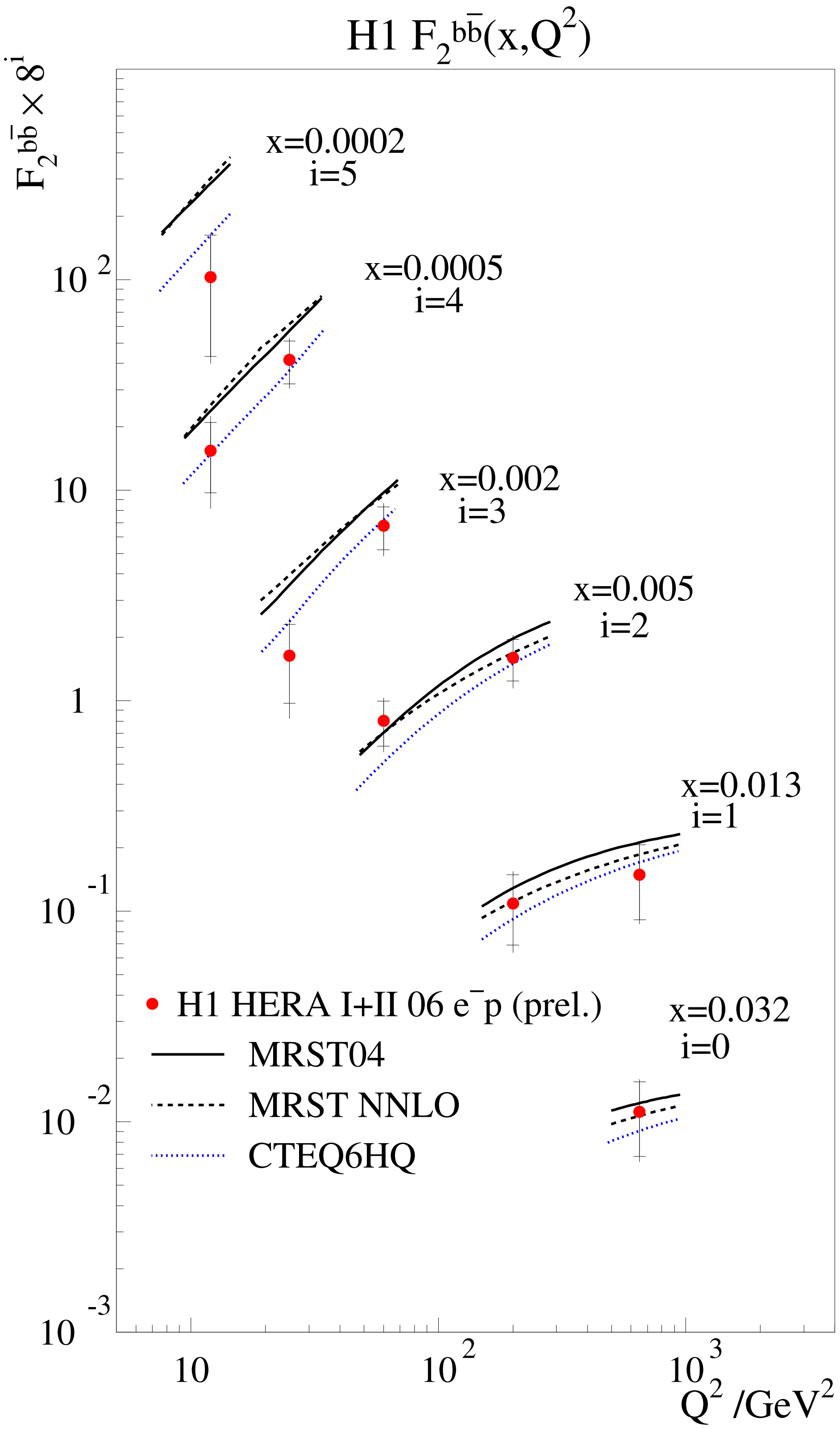

Figure 10: The measured HERA I and II averaged $F_2^{b\bar{b}}$ shown as a function of Q^2 for various x values. The inner error bars show the statistical error, the outer error bars represent the statistical and systematic errors added in quadrature. The predictions of QCD are also shown.

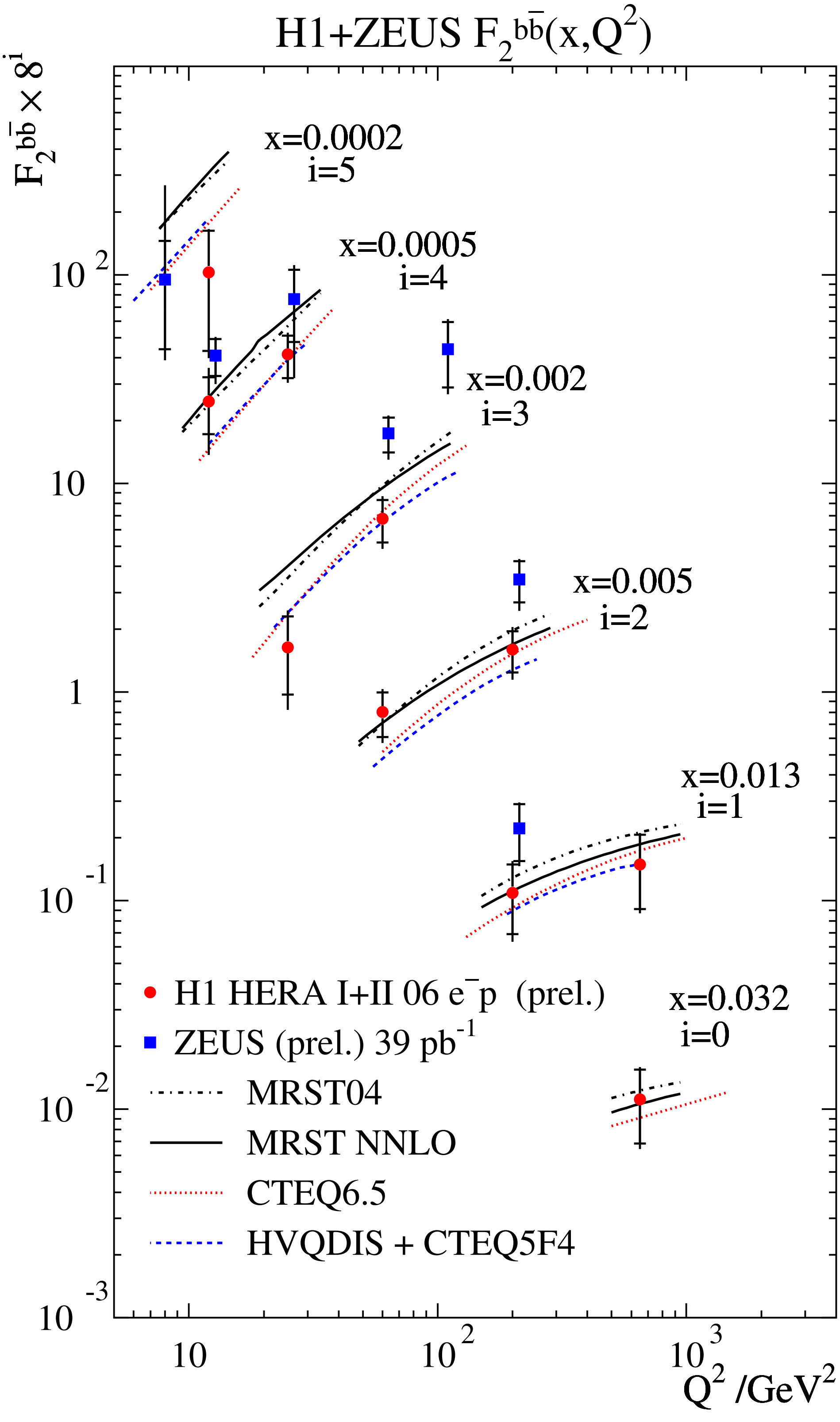

Figure 11: The measured HERA I and II averaged $F_2^{b\bar{b}}$ shown as a function of Q^2 for various x values. The inner error bars show the statistical error, the outer error bars represent the statistical and systematic errors added in quadrature. The preliminary data from ZEUS and predictions of QCD are also shown.